Electromechanical and Photoluminescence Properties of Al-doped ZnO Nanorods Applied in Piezoelectric Nanogenerators

Wen-Yang Chang · Te-Hua Fang · Ju-Hsuan Tsai

Abstract A piezoelectric nanogenerator based on Al-doped ZnO (AZO) nanorods with a V-zigzag layer is investigated at a low temperature. The growth temperature, growth time, growth concentration, photoluminescence (PL) spectrum, and AZO epitaxial growth on the ITO glass substrate using aqueous solution are reported and the associated electromechanical and PL properties are discussed. In general, the properties of piezoelectric nanogenerators and their functionality at ultralow temperatures (near liquid helium temperature) are important for applications in extreme environments. A V-zigzag layer is used to enhance the bending and compression deformation of the piezoelectric nanogenerator. The electromechanical properties of AZO nanorods are tested using an ultrasonic wave generator. Results show that the percent transmittance decreases with increasing growth time and growth temperature. The intensities of the PL spectrum and the (002) peak orientation increases with increasing growth temperature. AZO at a low growth temperature of 90 °C has good piezoelectric harvesting efficiency when the piezoelectric nanogenerator has a zigzag structure. The average current, voltage, and power density of the piezoelectric harvesting are $0.76\,\mu A$, 1.35 mV, and 1.026 nW/mm^2, respectively. These results confirm the feasibility of

W.-Y. Chang
Department of Mechanical and Computer-Aided Engineering, National Formosa University,
Yunlin 632, Taiwan

T.-H. Fang (✉)
Department of Mechanical Engineering, National Kaohsiung University of Applied Sciences,
415 Chien Kung Road, Sanmin District, Kaohsiung 807, Taiwan
e-mail: fang.tehua@msa.hinet.net

J.-H. Tsai
Institute of Electro-Optical and Materials Science, National Formosa University,
Yunlin 632, Taiwan

growing AZO at low temperature. AZO nanorods have potential for energy harvester applications.

Keywords Al dopant · ZnO · Nanogenerator · V-zigzag · Electromechanical · Photoluminescence

1 Introduction

Piezoelectric and dielectric properties have been extensively investigated at sintering [1] and liquid helium temperatures [2,3] and during radio-frequency (RF) magnetron sputtering [4]. Lead magnesium niobate-lead titanate single crystals (PMN-xPT) have excellent piezoelectric and dielectric properties at a liquid helium temperature of 4.2 K. Such investigations have primarily focused on phase transition behaviors, dielectric properties, and thermal conductivity [5]. Understanding piezoelectric behavior near the liquid helium temperature is important for advanced scientific research because quantum-mechanical effects control physical phenomena at these temperatures.

Semiconductor ZnO nanorods have been doped with group II and group III metal ions to enhance their nanostructural, optical, and electrical properties [6]. In general, pure zinc oxide (ZnO) nanorods have poor conductivity and lack stability in terms of thermal aging in air or corrosive environments [7]. Aluminum (Al)-doped ZnO (AZO) nanorod arrays have attracted attention in recent years due to their conductivity and transparency for applications in optoelectronic devices such as display panels, solar cells, and photovoltaic devices [8–10]. In addition, AZO nanorods have been demonstrated to exhibit an extremely stable field emission property [11] and are considered for transparent conductive electrodes [12] due to their high transparency, stability, and high conductivity. The c-axis orientation of AZO nanorods at the peak intensity of (002) was significantly enhanced compared to that at the peak of pure hexagonal ZnO [13].

Although the synthesis of ZnO nanorods has been extensively investigated [14–17], few works have reported the conductivity and transparency of AZO nanorods obtained via solution growth methods [18–21]. In addition, piezoelectric harvesting based on AZO nanorods has not been investigated in terms of the associated electromechanical and optical characteristics. Electron beam evaporation [22], pulsed-laser deposition [23], RF sputtering [24,25], spray pyrolysis [26], and the aqueous solution method have been used to synthesize AZO. The aqueous solution method is attractive because it can grow highly preferred-orientation ZnO nanorods and is suitable for optoelectronic fabrication at low cost [27].

This study proposes a piezoelectric harvester made of AZO nanorods that instantaneously transform their deformation into electrical energy. The growth temperature, growth time, growth concentration, photoluminescence (PL) spectrum, and AZO epitaxial growth effects on the ITO glass substrate using aqueous solution fabrication were investigated. The surface morphology, crystalline structure, and optical and electromechanical characteristics of AZO nanorods were analyzed. The feasibility of using AZO for harvester applications in electronics devices is demonstrated.

2 Experiments

2.1 AZO Preparation

AZO nanostructures on an ITO glass substrate mainly include a ZnO seed layer, a ZnO nanorod layer, and an Al doping layer. Each layer is described below.
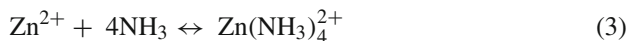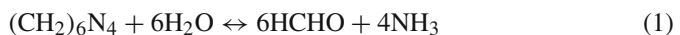
2.1.1 ZnO Seed Layer

The ZnO seed layer was fabricated using RF magnetron sputtering. Before the ZnO seed layer growth process, an ITO glass substrate was twice ultrasonically cleaned in deionized (DI) water, acetone, and then ethanol. A ZnO target with a purity of 99.99 % was then deposited on the ITO glass substrate via reactive sputtering deposition at a pressure of 6×10^{-6} Torr for 10 min. During the deposition of the seed layer, the RF power, rotation rate of the holder, cooling time, and gas flow ratio of argon to oxygen were 200 W, 25 rpm, 1 h, and 12:8, respectively. The distance from the ZnO target to the ITO glass substrate was about 10 cm. Finally, a ZnO seed layer with a thickness of about 20 nm was deposited on the ITO glass substrate.

2.1.2 ZnO Nanostructures

ZnO nanostructures were grown using zinc nitrate hexahydrate ($Zn(NO_3)_2$) and hexamethyltetramine (HMTA, $(CH_2)_6N_4$) aqueous solutions. Epitaxial ZnO nanostructures were then grown on the ZnO seed layer using a chemical aqueous solution method. During the chemical aqueous experiment, zinc nitrate hexahydrate was added into DI water under constant stirring until it had dissolved completely.

Ammonium hydroxide was then slowly added into the zinc nitrate hexahydrate solution. ZnO nanostructures were taken out of the zinc nitrate hexahydrate solution, rinsed using DI water, and dried at a temperature of about 50 °C. Hydroxide ions formed via the decomposition of HMTA; they reacted with Zn^{2+} to form ZnO. The second step was to grow ZnO nanorods from an aqueous solution at temperatures of 70, 80, 90, and 100 °C. The growth mechanism is shown in Fig. 1. The chemical reactions were as follows:
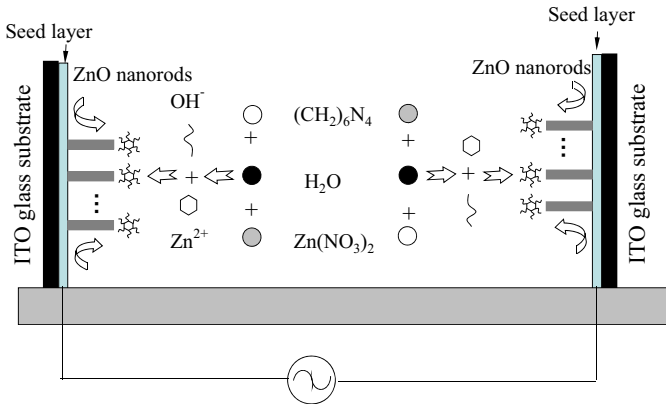
$$(CH_2)_6N_4 + 6H_2O \leftrightarrow 6HCHO + 4NH_3 \tag{1}$$

$$NH_3 + H_2O \leftrightarrow NH^{4+} + OH^- \tag{2}$$

$$Zn^{2+} + 4NH_3 \leftrightarrow Zn(NH_3)_4^{2+} \tag{3}$$

$$Zn(NH_3)_4^{2+} + 2OH^- \leftrightarrow Zn(OH)_2 + 4NH_3 \tag{4}$$

$$Zn(OH)_2 \leftrightarrow ZnO + H_2O \tag{5}$$

Fig. 1 Epitaxial ZnO growth mechanism at low temperature on ITO glass substrate (Color figure online)

2.1.3 Aluminum Doping Layer

AZO nanostructures were prepared using $Zn(NO_3)_2 \cdot 6H_2O$, $Al(NO_3)_3 \cdot 9H_2O$, and $(CH_3)_3Si \cdot NH \cdot Si(CH_3)_3$ in aqueous solution [28]. The concentrations of $Zn(NO_3)_2 \cdot 6H_2O$, HMTA, and $Al(NO_3)_3 \cdot 9H_2O$ were 0.1, 0.15, and 0.1 M, respectively, at a constant temperature of 90 °C at 4 h. After fabrication, the AZO samples were dried in an oven at a temperature of 80 °C for 2 h.

2.2 Piezoelectric Nanogenerator

In general, conventional energy harvesters made of piezoelectric materials are fabricated as bulk, film, or block forms [29]. However, piezoelectric nanorod arrays with a V-zigzag structure have higher energy conversion efficiency due to their larger geometrical strain-to-area ratio [14]. The V-zigzag structure provides a normal stress and a bending moment to efficiently convert piezoelectric vibrations into energy harvesting due to higher electromechanical coupling [14]. AZO nanotubes with a V-zigzag structure with an electrode pitch of 3 μm are shown in Fig. 2. The V-zigzag electrodes and AZO nanorods are initially closed. Piezoelectric characteristics of AZO are then been generated by applying external forces. The V-zigzag structure is based on a standard (100) silicon wafer with a diameter of 4 inches (10.16 cm). For V-zigzag structure fabrication, a silicon nitride film was firstly deposited on the silicon wafer surface. The wafer was placed in a special holder and KOH was used to partially etch the backside for the V-zigzag layer. The final step was to grow an electrode with a thickness of about 0.1 μm.

2.3 Characteristic Analysis

The crystallinity and orientation of the piezoelectric structures were examined using X-ray diffraction (XRD, MO3XHF22, MAC-Science). The PL spectra of the piezo-
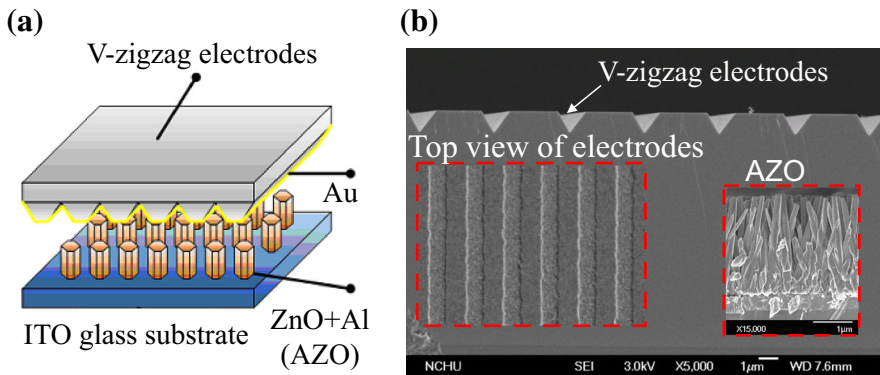
(a)

(b)

Fig. 2 Energy harvesting mechanism based on V-zigzag electrodes and AZO nanorods, **a** AZO and V-zigzag structures, **b** SEM pictures (Color figure online)

electric structure were obtained using a fluorescence spectrophotometer (F-4500, Hitachi) with an excitation wavelength of 300 nm. The surface morphology of the AZO samples was investigated using field-emission scanning electron microscopy (SEM, JEOL JSM-7401F). The piezoelectric nanorods were excited using monochromic light with a wavelength resolution of 1.5 nm and a 150-W xenon lamp at room temperature. A 350-nm filter was used to obtain the real emission of the AZO nanotubes. The crystalline phases and surface properties of the AZO nanotubes at various growth times, temperatures, and concentration ratios were investigated.

3 Results and Discussion

The effects of growth time, growth temperature, concentration ratio, and Al doping on ZnO epitaxial piezoelectric characteristics are discussed below.

3.1 Effect of Growth Time

PL spectra of ZnO nanorods obtained at growth times of 1, 4, 8, and 13 h at a temperature of 80 °C and a 1:4 concentration ratio of zinc nitrate hexahydrate to hexamethylenetetramine are shown in Fig. 3a. The PL spectra of ZnO nanorods exhibit near-band-edge emission at a wavelength of 398 nm with a full width at half maximum (FWHM) of 18 nm. The intensity of the PL spectrum increased with increasing growth time, except for a growth time of 13 h. The ZnO nanorods obtained at a growth time of 8 h had the strongest PL spectrum intensity. The wavelength of the maximum intensity at the first peak is about 398 nm. There is a broad band at a wavelength of around 425 nm, which can be attributed to oxygen vacancies [29].

The surface morphologies of ZnO nanorods grown at 1, 8, and 13 h are shown in the inset of Fig. 3a. For a growth time of above 4 h, the ZnO nanorods exhibited a hexagonal shape and were well-aligned perpendicular to the ITO substrate surface along the c-axial growth direction. This indicates that epitaxial ZnO can outgrow itself

Fig. 3 Characteristics of ZnO nanorods obtained at growth times of 1, 4, 8, and 13 h at 80 °C and a concentration ratio of 1:4 of zinc nitrate hexahydrate to hexamethylenetetramine. a PL spectra, b XRD patterns, and c percent transmittance (Color figure online)
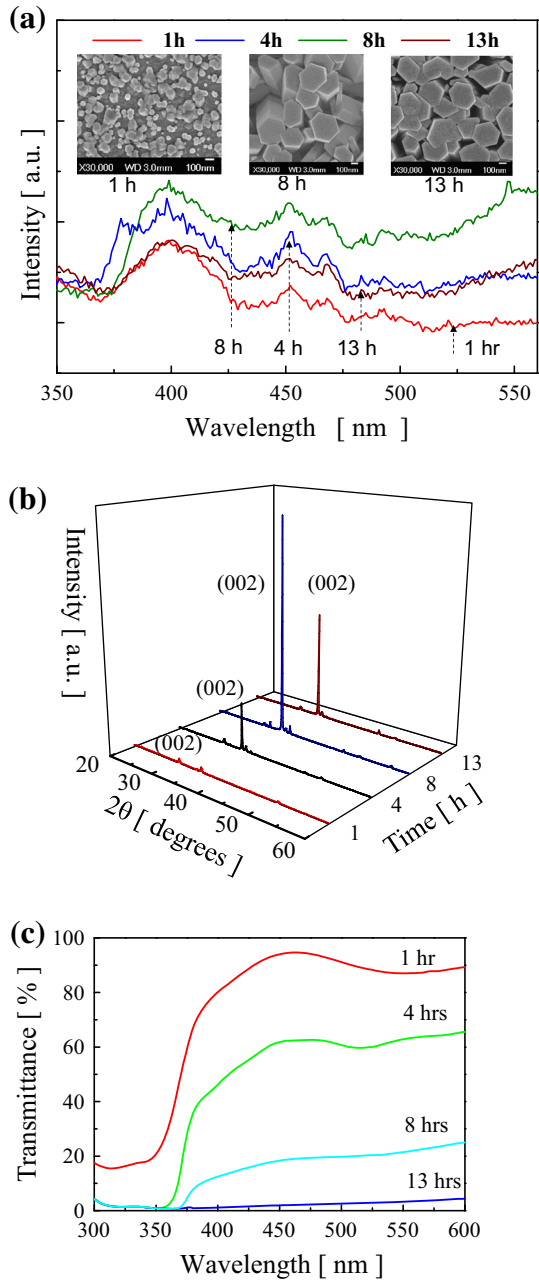
along the c-axial growth direction at a growth time of above 8 h, but reaches super-saturation at a growth time of 13 h. The diameter and length of the ZnO nanorods increased with increasing synthesis time. The diameters of ZnO nanorods synthesized

for 1, 4, 8, and 13 h are 80.2, 198.6, 255.4, and 352 nm, respectively. The lengths of these ZnO nanorods are 78.2, 628.0, 3300, and 2980 nm, respectively.

Figure 3b shows the XRD patterns of ZnO nanorods obtained at growth times of 1, 4, 8, and 13 h. An extra peak appears at about 34.4° in the XRD pattern in the 2θ range at a growth time of 8 h. The extra peak corresponds to the (002) orientation of the c-axis. The (002) orientation of zinc oxide indicates that the c-axis was oriented normally to the ITO substrate surface. The intensity of the (002) peak increased with increasing growth time. In general, a good crystalline structure of ZnO exhibits a strong intensity and a narrow FWHM. The maximum value of the (002) intensity peak appeared at a growth time of 8 h. However, the (002) intensity peak of epitaxial ZnO growth was restrained when the growth time was 13 h. This is due to the degree of super-saturation being lowered with time.

Figure 3c shows the percent transmittance of ZnO nanorods obtained at growth times of 1, 4, 8, and 13 h. The percent transmittance, $T(\%)$, was determined as $(I_t/I_0) \times 100\%$, where I_0 and I_t are the input intensity and transmittance intensity of a monochromatic beam, respectively. The results show that the percent transmittance decreased with increasing growth time. The maximum values of percent transmittance of ZnO nanorods obtained at growth times of 1, 4, 8, and 13 h are 94.7, 65.5, 25, and 4.4 %, respectively. The ZnO nanostructures obtained at a growth time of over 13 h did not transmit. The absorption edges shifted toward lower wavelengths with decreasing growth time. In contrast to the Burstein–Moss effect, the band edge absorption has a blue shift with decreasing thickness [30–32]. The blue and violet shifts of transmittance near the band edge are likely due to the quantum confinement effect.

3.2 Effect of Growth Temperature

ZnO nanorods grown at temperatures of 70, 80, 90, and 100 °C for 4 h at a concentration ratio of 1:4 of zinc nitrate hexahydrate to hexamethylenetetramine were investigated, as shown in Fig. 4a. The intensity of the PL spectrum increased with increasing growth temperature. The PL spectrum trends are similar for growth temperatures of above 90 °C. For growth temperatures of above 70 °C, the ZnO nanostructures were uniformly distributed across the entire ITO substrate. The ZnO nanorod tops had a hexagonal shape, with the c-axis perpendicular to the ITO substrate surface. The lengths of ZnO nanorods obtained at growth temperatures of 70, 80, 90, and 100 °C are 0.47, 0.98, 1.81, and 2.5 µm, respectively. The ZnO structures obtained at growth temperatures of above 100 °C had needle-like and sparse morphologies, as shown in the inset of Fig. 4a. The needle-like morphology reflects the structure of the ZnO lattice, elongated in the c-axis direction with hexagonal prismatic faces. It can be predicted that the growth velocity of ZnO nanorods in the longitudinal direction is faster than that in the transverse direction when the growth temperature is above 100 °C. According to surface morphologies, the growth velocity of ZnO nanorods in the transverse direction gradually increased with increasing growth time.

Figure 4b shows the XRD patterns of ZnO nanorods grown at temperatures of 70, 80, 90, and 100 °C. There is no peak at the (002) orientation for the growth temperature of 70 °C, indicating that the activation barrier for ZnO growth cannot be overcome below

Fig. 4 Characteristics of ZnO nanorods obtained at growth temperatures of 70, 80, 90, and 100 °C at a growth time of 4 h and at a concentration ratio of 1:4 of zinc nitrate hexahydrate to hexamethylenetetramine. **a** PL spectra, **b** XRD patterns, and **c** percent transmittance (Color figure online)
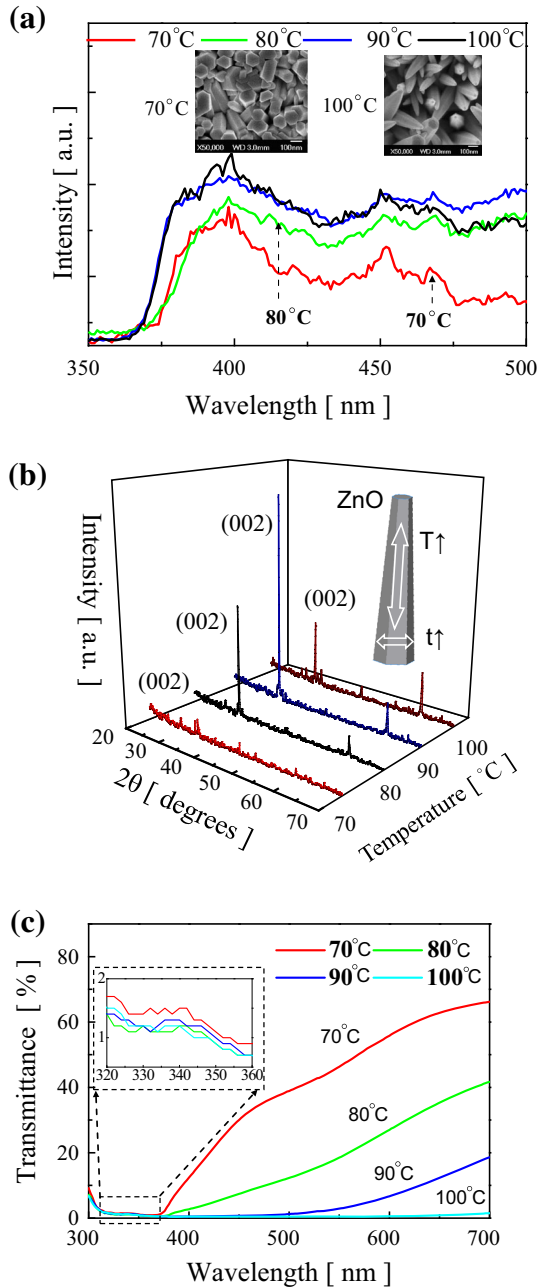
this temperature. The intensity of the (002) peak orientation increased with increasing growth temperature. The maximum intensity value appeared at 90 °C. The (002) peak intensity of epitaxial ZnO growth was restrained when the growth temperature was over 100 °C.

Figure 4c shows the percent transmittances of ZnO nanostructures obtained at growth temperatures of 70, 80, 90, and 100 °C. Results show that the ZnO nanostructures did not transmit in the wavelength range of 300–400 nm regardless of the growth time used for synthesis. The maximum values of percent transmittances of ZnO nanostructures obtained at growth temperatures of 70, 80, 90, and 100 °C are 66.2, 41.7, 18.6, and 6.8 %, respectively. The ZnO nanostructures did not transmit when the growth temperature was 100 °C.

### 3.3 Concentration Ratio and Al Dopant Effect

ZnO nanorods synthesized with concentration ratios of 1:1, 1:2, 1:3, 1:4, and 1:5 of zinc nitrate hexahydrate to hexamethylenetetramine at 90 °C for 4 h were investigated. The AZO nanostructures were prepared using $Zn(NO_3)_2 \cdot 6H_2O$, $Al(NO_3)_3 \cdot 9H_2O$, and $(CH_3)_3Si \cdot NH \cdot Si(CH_3)_3$ in aqueous solution at a constant temperature of 90 °C for 4 h. Figure 5a shows the PL spectra of the synthesized ZnO nanorods. Only two peaks, in the ranges of 380–420 and 520–570 nm, respectively, appeared. The intensity of the visible luminescence band gradually decreased when the concentration ratio was increased. However, the intensity peak at the wavelength of 550 nm remarkably increased at a growth concentration ratio of 1:5 due to the quantum confinement effect. A PL comparison of AZO obtained at a concentration ratio of 1:5, a growth time of 8 h, and a growth temperature of 90 °C is shown in Fig. 5b. The intensity peak of AZO spectrum at the wavelength of 400 nm remarkably is higher than others. However, the intensity peak of AZO spectrum at the wavelength of 550 nm remarkably is lower compared to others due to a decrease in the band energy.

The ZnO nanostructures were needle-like when the concentration ratio was below 1:2, as shown in the inset of Fig. 5b. In general, Al should have no significant influence on ZnO structures. Al doping of ZnO structures can decrease the electrical resistivity and increase the electron Hall mobility, which benefit piezoelectric energy harvesting. The electrical resistivity of the AZO thin films slightly decreased with increasing aspect ratio of nanorods, and their mobility significantly increased with increasing length. The lengths of ZnO nanorods obtained at concentration ratios of 1:2, 1:3, 1:4, and 1:5 are 0.97, 1.15, 1.21, and 2.25 μm, respectively. The fast increase of ZnO length at the concentration ratio of 1:5 is likely due to HMTA quickly releasing NH_3. However, it is worth noting that Al doping had no significant influence on the length of ZnO nanorods. The XRD patterns of ZnO nanorods grown at various concentration ratios are shown in Fig. 5c. The intensity of the (002) peak orientation increased with increasing concentration ratio. The maximum value appeared at the concentration ratio of 1:5. The maximum values of percent transmittances of ZnO nanostructures obtained at concentration ratios of 1:2, 1:3, 1:4, and 1:5 are 45.5, 40.6, 33.5, and 28.8 %, respectively.

3.4 Piezoelectric Nanogenerator

The growth conditions of AZO nanorods for a piezoelectric nanogenerator were as follows: a concentration ratio of 1:5 of zinc nitrate hexahydrate to hexamethylenete-

Fig. 5 Characteristics of ZnO nanorods obtained at growth concentration ratios of 1:1, 1:2, 1:3, 1:4, and 1:5 of zinc nitrate hexahydrate to hexamethylenetetramine at 90 °C for 4 h. **a** PL spectra, **b** PL comparisons of AZO, and **c** XRD patterns (Color figure online)
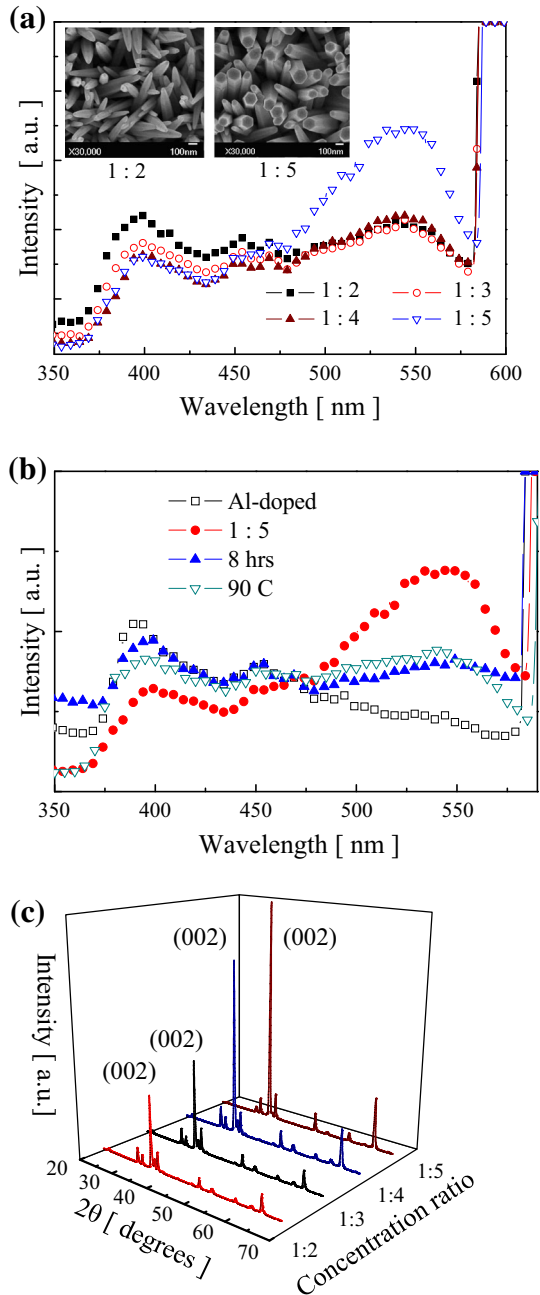
tramine, a growth time of 4 h, and a growth temperature of 90 °C. The piezoelectric nanogenerator was based on V-zigzag electrodes and AZO structures. It was packaged in a thermoplastic poly(ethylene terephthalate) (PET) membrane with a thickness of
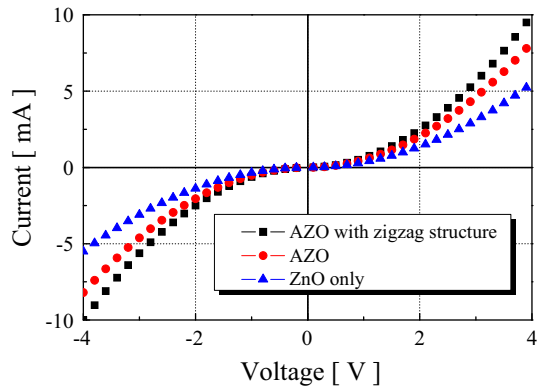
80 μm using a hot press. Energy harvesting was measured using a digital multimeter (Keithley 2400) and in DI water using an ultrasonic wave generator with a frequency of 43 kHz and a power of 50 W. In general, one-dimensional nanorods have much larger length-to-diameter and surface-to-volume ratios than those of piezoelectric materials in bulk, film, or block forms. During energy harvesting, the V-zigzag layer generates a normal stress and a bending moment to vibrate the AZO nanorods via ultrasonic wave vibration.

Figure 6a shows the current–voltage (I–V) characteristics of ZnO nanorods, AZO nanorods, and AZO nanorods with a zigzag structure. The harvesting current increased with increasing applied voltage for all nanogenerators. These nanogenerators exhibited Schottky-like I-V characteristics and constructively generated harvesting currents. In general, a Schottky-like barrier is at a forward bias if the piezoelectric nanogenerator has a high potential, otherwise it is reverse biased. The harvesting efficiency followed the sequence AZO with zigzag structures > AZO > ZnO.

For piezoelectric harvesting, ZnO nanorods and AZO nanorods generate lower current responses compared to those of AZO with zigzag structures at a given voltage. AZO with zigzag structures has good piezoelectric harvesting efficiency due to its relatively large deformation [33]. The transfer efficiency of AZO with zigzag structures for energy harvesting was about 19 % higher than that for AZO. For energy harvesting at an applied voltage of 4 V, the harvesting percentages of AZO with zigzag structures and AZO are 49 and 82 % higher than that of ZnO nanorods, respectively.

Figure 7a, b show the currents and voltages of reproducible energy harvesting after an ultrasonic wave generator was turned on or off, respectively. The effective area and the power density of the AZO energy harvesting are about 50 mm^2 and 1.026 nW/mm^2, respectively. The current and voltage of the average harvesting outputs were 0.76 μA and 1.35 mV, respectively, when the ultrasonic wave generator was turned on. The current and voltage responses of AZO had small perturbation of the energy harvesting during the steady state. Therefore, the V-zigzag structures efficiently convert piezoelectric vibrations into energy harvesting due to their higher electromechanical coupling after the application of external forces. AZO with zigzag structures has a low aspect ratio and low packing density, making it suitable for piezoelectric nanogenerator applications.
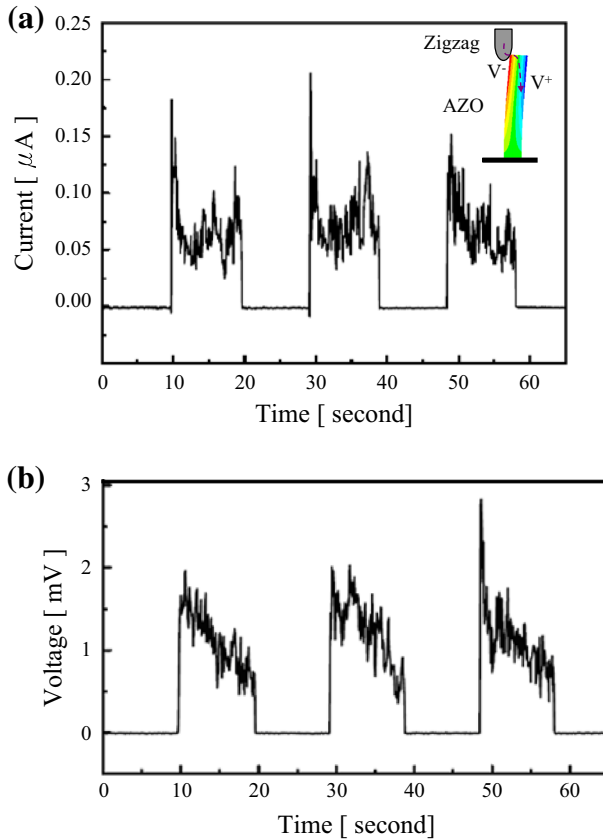
Fig. 7 Piezoelectric harvesting with AZO using ultrasonic wave generator that was turned on or off. **a** Current and **b** voltage responses (Color figure online)

4 Conclusion

AZO nanorods with a V-zigzag layer for piezoelectric harvesting were demonstrated at a low temperature. The efficiency of energy harvesting increased by about 19 % when the V-zigzag structures were used to make contact with AZO nanorods. For a growth time of 4 h, ZnO nanorods had a hexagonal morphology and were perpendicularly aligned to the ITO glass substrate along the *c*-axial growth direction. There was no peak at the (002) orientation for a growth temperature of 70 °C, indicating that temperatures of below 70 °C are unsuitable for growing structures with piezoelectric characteristics. AZO nanorods with a well-orientation (002) had the highest intensity when synthesized at a concentration ratio of 1:5 of zinc nitrate hexahydrate to hexamethylenetetramine for 4 h at 90 °C. The piezoelectric harvester made of AZO nanorods exhibited Schottky-like I-V characteristics. The results could provide useful information for touch panel and large-area electronics harvesting device applications.

References

1. S.Y. Yeon, J.H. Yoon, S.Y. Jin, J.C. Won, High-power properties of piezoelectric hard materials sintered at low temperature for multilayer ceramic actuators. J. Eur. Ceram. Soc. **33**(1), 1769–1778 (2013)
2. V.P. Mineev, Half-quantum vortices in polar phase of superfluid He-3. J. Low Temp. Phys. **177**(1–2), 48–58 (2014)
3. J.B. Ketterson, Probing the frequency and wavevector dependent response of 3He using patterned piezoelectric transducers. J. Low Temp. Phys. **159**(5–6), 606–613 (2010)
4. Q. Chen, T. Wang, J. Wu, X. Cheng, X. Wang, B. Zhang, D. Xiao, J. Zhu, Low temperature sintering of $Ba_0.91Ca_0.09Ti_0.916Sn_0.084O_3$ lead-free piezoelectric ceramics with the additives of ZnO and MnO_2. J. Electroceram. **32**(2–3), 175–179 (2014)
5. G. Wei, J. Dafei, W. Wanchun, J.M. Humphrey, Low temperature piezoelectric and dielectric properties of lead magnesium niobate titanate single crystals. J. Appl. Phys. **102**, 084104 (2007)
6. T.A. El-Brolossy, O. Saber, S.S. Ibrahim, Determining the thermophysical properties of Al-doped ZnO nanoparticles by the photoacoustic technique. Chin. Phys. B **22**(1), 074401 (2013)
7. A.E. Jimenez-Gonzalez, Modification of ZnO thin films by Ni, Cu, and Cd doping. J. Solid State Chem. **28**(2), 176–180 (1997)
8. O. Bamiduro, H. Mustafa, R. Mundle, R.B. Konda, A.K. Pradhan, Metal-like conductivity in transparent Al:ZnO films. Appl. Phys. Lett. **90**(25), 252108–252110 (2007)
9. P. Kadam, C. Agashe, S.J. Mahamuni, Al-doped ZnO nanocrystals. J. Appl. Phys. **104**(10), 103501–103501-4 (2008)
10. K.Y. Wu, C.C. Wang, D.H. Chen, Preparation and conductivity enhancement of Al-doped zinc oxide thin films containing trace Ag nanoparticles by the sol-gel process. Nanotechnology **18**(30), 305604 (2007)
11. X.Y. Xue, L.M. Li, H.C. Yu, Y.J. Chen, Y.G. Yang, Extremely stable field emission from AlZnO nanowire arrays. Appl. Phys. Lett. **89**(4), 043118 (2006)
12. B.H. Kong, M.K. Choi, H.K. Cho, J.H. Kim, S. Baek, J.H. Lee, Conformal coating of conductive ZnO:Al films as transparent electrodes on high aspect ratio Si microrods. Electrochem. Solid State Lett. **13**(2), K12–K14 (2010)
13. S. Mondal, K.P. Kanta, P. Mitra, Preparation of Al-doped ZnO AZO thin film by SILAR. J. Phys. Sci. **12**(1), 221–229 (2008)
14. W.Y. Chang, T.H. Fang, C.I. Weng, S.S. Yang, Flexible piezoelectric harvesting based on epitaxial growth of ZnO. Appl. Phys. A **102**(3), 705–711 (2010)
15. Y. Zhou, W. Wu, G. Hu, H. Wu, S. Cui, Hydrothermal synthesis of ZnO nanorod arrays with the addition of polyethyleneimine. Mater. Res. Bull. **43**(8–9), 2113–2118 (2008)
16. K. Elen, H.V. den Rul, A. Hardy, M.K.V. Bael, J. DHaen, R. Peeters, D. Franco, J. Mullens, Hydrothermal synthesis of ZnO nanorods: a statistical determination of the significant parameters in view of reducing the diameter'. Nanotechnology **20**(5), 055608 (2009)
17. S.K. Park, J.H. Park, K.Y. Ko, S. Yoon, K.S. Chu, W. Kim, Y.R. Do, Hydrothermal-electrochemical synthesis of ZnO nanorods. Cryst. Growth Des. **9**(8), 3615–3620 (2009)
18. J. Kim, J.H. Yun, S.W. Jee, Y.C. Park, M. Ju, S. Han, Y. Kim, J.H. Kim, W.A. Anderson, J.H. Lee, J. Yi, Rapid thermal annealed Al-doped ZnO film for a UV detector. Mater. Lett. **65**(4), 786–789 (2011)
19. Z. Zhan, J. Zhang, Q. Zheng, D. Pan, J. Huang, F. Huang, Z. Lin', Strategy for preparing Al-doped ZnO thin film with high mobility and high stability. Cryst. Growth Des. **11**(1), 21–25 (2011)
20. S. Cho, S.H. Jung, J.W. Jang, E. Oh, K.H. Lee, Simultaneous synthesis of Al-doped ZnO nanoneedles and zinc aluminum hydroxides through use of a seed layer. Cryst. Growth Des. **8**(12), 4553–4558 (2008)
21. W.Y. Chang, T.H. Fang, C.-H. Syu, Material characteristics of zinc oxide doped aluminum for micro-harvesting. Appl. Mech. Mater. **80–81**(1), 245–249 (2011)
22. J. Ma, F. Ji, D.H. Zhang, H.L. Ma, S.Y. Li, Optical and electronic properties of transparent conducting ZnO and ZnO:Al films prepared by evaporating method. Thin Solid Films **357**(1), 98–101 (1999)
23. Y. Liu, J. Lian, Optical and electrical properties of aluminum-doped ZnO thin films grown by pulsed laser deposition. Appl. Surf. Sci. **253**(7), 3727–3730 (2007)
24. X.J. Wang, Q.S. Lei, W. Xu, W.L. Zhou, J. Yu, Preparation of ZnO:Al thin film on transparent TPT substrate at room temperature by RF magnetron sputtering technique. Mater. Lett. **63**(16), 1371–1373 (2009)

25. K.H. Kim, R. Wibowo, A.B. Munir, Properties of Al-doped ZnO thin films sputtered from powder compacted target. Mater. Lett. **60**(15), 1931–1935 (2006)
26. A.F. Aktaruzzaman, G.L. Sharma, L.K. Malthotra, Electrical, optical and annealing characteristics of ZnO:Al films prepared by spray pyrolysis. Thin Solid Films **198**(1–2), 67–74 (1991)
27. Y.T. Yin, W.X. Que, C.H. Kam, ZnO nanorods on ZnO seed layer derived by sol–gel process. J. Sol-Gel Sci. Technol. **53**(3), 605–612 (2010)
28. T.H. Fang, S.H. Kang, Physical properties of ZnO:Al nanorods for piezoelectric nanogenerator application. Curr. Nanosci. **7**(1), 505–511 (2010)
29. W.Y. Chang, C.H. Yang, Energy harvesting simulation of piezoelectric ZnO for electromechanical nanogenerators. Adv. Energy Eng. **1**(1), 102–107 (2013)
30. W.L. Wu, G.G. Siu, C.L. Fu, H.C. Ong, Photoluminescence and cathodoluminescence studies of stoichiometric and oxygen-deficient ZnO films. Appl. Phys. Lett. **78**(1), 2285–2287 (2001)
31. Water W., Fang T. H., Ji L. W., Lee C. C., Effect of growth temperature on photoluminescence and piezoelectric characteristics of ZnO nanowires. Mater. Sci. Eng. B **158**(1–3), 75–78 (2009)
32. H.M. Kim, S.K. Jung, J.S. Ahn, Y.J. Kang, K.C. Je, Electrical and optical properties of in2o3-ZnO films deposited on polyethylene terephthalate substrates by radio frequency magnetron sputtering. Jpn. J. Appl. Phys. **42**(1), 223–227 (2003)
33. X. Wang, J. Song, J. Liu, Z.L. Wang, Drect-current nanogenerator driven by ultrasonic waves. Science **316**(1), 102–105 (2007)